COVER SHEET

Paper Number: **262**

Title: **Progressive Damage Failure Analysis of Post-Buckled Composite Single-Stringer Panel with Teflon Inserts**

Authors: Vijay K. Goyal*
Austin Pennington
Jason Action

*Corresponding author

All pages must have the following:

(FIRST PAGE OF ARTICLE – *align this to the top of page – leave space blank above ABSTRACT*)

ABSTRACT

The high strength-to-weight and stiffness-to-weight ratio materials, such as laminated composites, are advantageous for modern aircraft. Laminated composites with initial flaws are susceptible to delamination under buckling loads. PDA tools help enhance the industry's understanding of the mechanisms for damage initiation and growth in composite structures while assisting in the design, analysis, and sustainment methods of these composite structures. The global-local modeling approach for the single-stringer post-buckled panel was evaluated through this effort, using Teflon inserts to simulate the defect of damage during manufacturing. This understanding is essential for designing the post-buckled structure, reducing weight while predicting damage initiation location, and addressing a potential design review for future aircraft repairs. In this work, the initial damage was captured with Teflon inserts as the starting configuration; and any reference to the damage initiation refers to any damage beyond the "initial unbonded region." The effort aims to develop, evaluate, and enhance methods to predict damage initiation and progression and the failure of post-buckled hat-stiffened panels using multiple Abaqus FEA Virtual Crack Closure Technique (VCCT) definitions. Validation of the PDA using the VCCT material model was performed on a large single-stringer panel subjected to compressive loading. The compressive loading of the panel caused the skin to buckle before any damage began to occur locally. In addition, comparisons are made for critical aspects of the damage morphology, such as a growth pattern that included delamination from the skin-stiffener interface to the skin and ply interfaces. When compared against the experimental data produced through the NASA Advanced Composites Project (ACP), the present model captured damage migration from one surface to another, and model validations were within 4% of the experimental data.

_____

Vijay K. Goyal, Lockheed Martin Aeronautics, Marietta, U.S.A
Austin Pennington, Lockheed Martin Aeronautics, Fort Worth, TX, U.S.A
Jason Action, Lockheed Martin Aeronautics, Marietta, GA, U.S.A

INTRODUCTION

Composite materials in aerospace structures have experienced a significant increase in use due to their high specific strength, lightweight, resistance to fatigue and corrosion, and their ability to be tailored for various designs. Mainly, composite skin-stiffened panels are a dominant part of airframes because of their excellent anti-buckling capabilities, significantly improving structural stability. In addition, these stiffened panels perform outstandingly in the nonlinear post-buckled region (behavior Through experimental work (Degenhardt et al. [1]; Hao et al. [2]; Gliszczynski et al. [3]). However, identifying damage initiation and progression of post-buckled composite stiffened panels under compression is a challenging event (Pietropaoli and Riccio [4]; Gong et al. [5]; Gong et al. [6]).

Typical composite bonded stiffened panels can withstand the post-buckling regime. However, their failure prediction is quite challenging because of the interaction of the post-buckling deformation with different failure modes, such as intralaminar damage, delamination, skin-stiffener delamination (Bisagni et al. [7]; Anyfantis and Tsouvalis [8]). Delamination, particularly the separation of the skin-stiffener and ply-ply, is the most common and critical damage in stiffened panels. Delamination propagation is considered a crack propagation problem, and several methods have been proposed to capture this behavior. On such method is the Virtual Crack Closure Technique (VCCT) and has been widely used by several authors (De Carvalho et al. [9]; Mabson et al. [10]; Di Memmo and Bisagni [11]; Raimondo et al. [12]; Camanho et al. [13]).

The purpose of this methodology is to use multiple VCCT definitions within Abaqus to capture the post-buckled damage of laminated composite hat-stiffened panels. The model will be validated with experimental data conducted through the NASA Advanced Composites Project (ACP) (Leone et al. [14]; Leone et al. [15]). The experimental models subjected to static compression loading were: (i) Panel with a pristine condition (no flaw), (ii) Panel with a known flaw (Teflon insert), and (iii) panel with initial impact damage. This paper addresses the single stringer with a Teflon insert to model an embedded flaw.

TESTING CONFIGURATION

This work focused on hat-stiffened panels designed to carry the load into a post-buckled state and were fabricated and tested under the NASA ACP. The panel measured 20.20-inches in length and 8.18-inches in width and consisted of IM7-8552 unidirectional tape with a layup of $[-45/45/0/90/-45/45/]_S$ where the 0-degree orientation was in the direction of the specimen length, shown in Figure 1. A 1.40-inch tall and 4.25-inch wide composite hat stiffener made of IM7/8552 plain weave (PW) fabric was cocured along with the panel. The hat was composed of an inner-wrap of $[45/-45/0/45]_T$ (inside to out), an outer-wrap of $[45/-45/0/45/45/0/-45/45/45/-45/0/45]_T$ (bottom to top), and a filled noodle region where the two ply-wraps diverge from one another. The noodle was assumed to be filled with 8552 epoxy. Tabs of the same material and layup of the skin panel were bonded to the panel ends to create

symmetric pad-up regions and a 10:1 ramp-down to the main skin region. These pad-ups acted to promote buckling and failure away from the specimen boundary conditions.

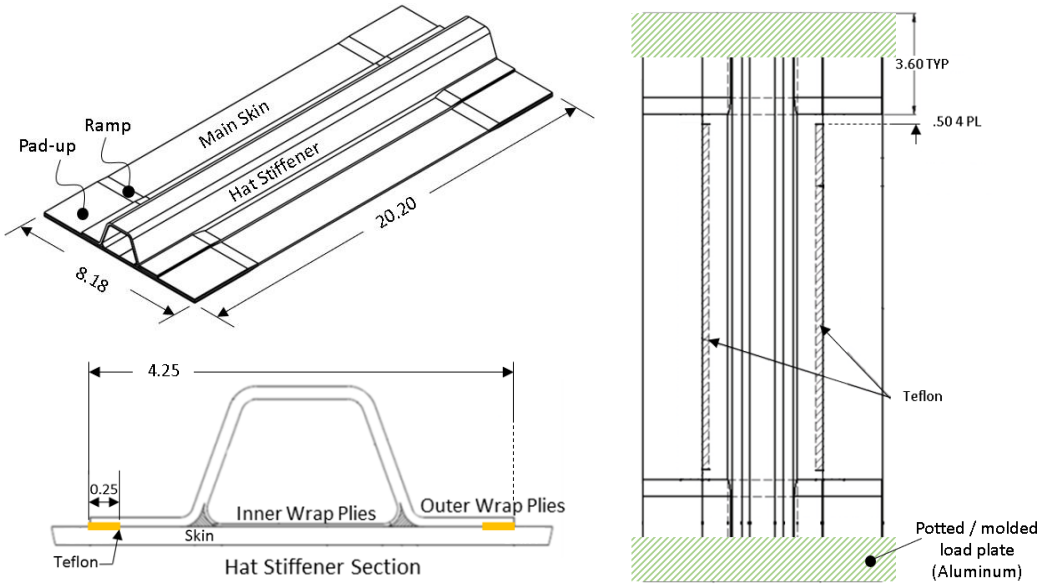

Figure 1. Panel Geometry

The panels were loaded in pure axial compression using a 100-kip servo-hydraulic load frame well past their critical buckling load into the post-buckling regime. The ends of the panels were potted with an adhesive material bonding them to a molded Aluminum load plate, which enforced zero rotation boundary conditions at the ends. The test aimed to induce debonding between the hat stiffener and skin panel near the center of the specimen. This delamination was initiated due to out-of-plane tensile stresses induced by the panel's tendency to deflect away from the stiffener in its buckled shape. To this end, 0.25-inch wide PTFE (Teflon) strips were included in the co-cured assembly between the hat-to-skin interfaces at the edge of the hat flanges and were terminated 0.50-inches from the ramp-down terminations.

Table 1. Test Results Summary

Specimen	# Runs	Buckling Mode	First AE [kips]	Peak Load [kips]
F-SSC-02	3	Type A		-34.1
F-SCC-01	1	Type B	-24	-30.5
F-SCC-04	5	Type B		-30.6

Three identical specimens were tested to failure, which consisted of catastrophic separation of the hat stiffener from the buckled skin panel. Table 1 shows that one of the specimens buckled in a "Type A" mode shape, and the remaining two buckled in a "Type B" shape. The "Type B" shape consisted of three half-waves in the panel of a down, up, down behavior, where a downward deflection indicates being away from

the stiffener. This deflection pattern was almost symmetric about the lengthwise midline of the specimen, with a maximum deflection at the edges of the panel width, as shown in Figure 2. Type A refers to a shape with opposite direction deflections as Type B. The specimens which buckled in the Type B shape were chosen for model correlation as they exhibited a lower failure load than the specimen which buckled in a Type A shape, an average of -30.6 kips. Of these two specimens, one was loaded uninterrupted to failure, while the other was loaded incrementally, with ultrasound (UT) and x-ray computed tomography (CT) scans taken between loadings to document states of stable progressive damage between initiation and final failure. In this specimen, the first unloading and scanning took place at -28.6 kips, at which damage progression had already taken place. In specimen F-SCC-01, which was loaded to failure without intermediate scans, acoustic emission was recorded at a load of -24 kips. Damage initiation could have occurred earlier and gone undetected. These two data points suggest that damage initiation occurred somewhere between -24 kips and -28.6 kips, being the range of detectable damage using the techniques employed on these tests. Damage was observed as delamination between the skin and hat, the first skin interface, and matrix cracking in the first skin ply. During testing, additional damage was observed to have migrated into the second skin interface (ply2-ply3) just before or during the final failure, but this work did not focus on it. This was due to the assumption that this was a secondary failure mode and was not a primary driver of the peak load of the specimen.

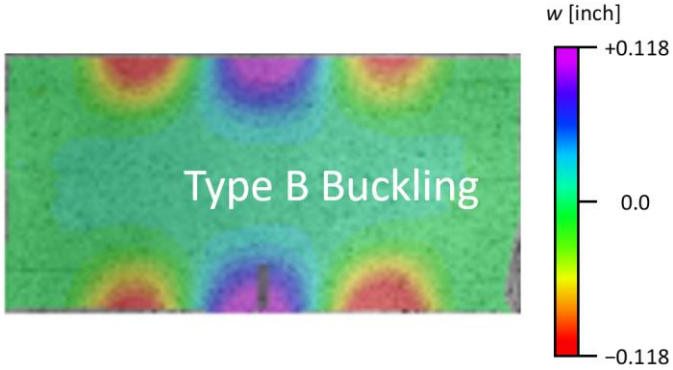

Figure 2. Digital Image Correlation (DIC) Plot of Out-of-Plane Deflections for Skin Panel Buckled Shape

INTERLAMINAR FAILURE PREDICTION USING VCCT

The finite element model (FEM) was completed in Abaqus/CAE to model and visualize results. Figure 3 shows the meshes of the skin-hat perimeter and middle regions were tied together to allow uncoupled refinement of these regions. The virtual crack closure technique (VCCT) was chosen as the progressive damage analysis (PDA) method to simulate debonding between layers in the refined region of the model. The skin-hat perimeter meshes were defined with one continuum shell element (SC8R) through the thickness everywhere but the pad-up and ramp, which

had two. The element in-plane dimensions were a maximum of 0.25-inches. The hat inner-wrap and over-wrap were both assigned one element through the thickness. The composite layup was explicitly defined for all skin and hat regions except the hat noodle, meshed with continuum solid C3D8R elements with an isotropic material property corresponding to IM7-8552 epoxy.

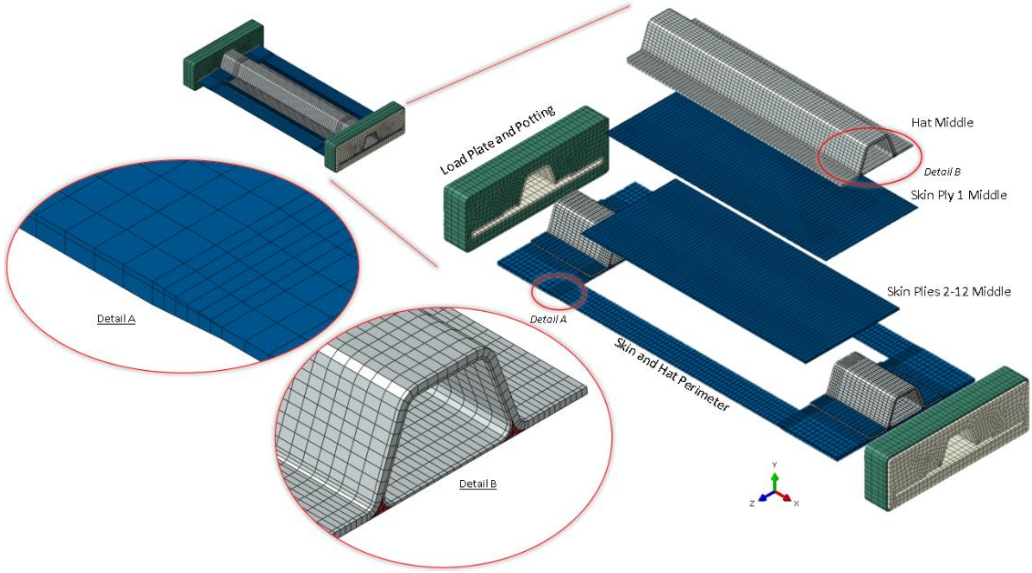

Figure 3. Finite Element Model General Arrangement

Testing indicated that debonding occurred in the flange of the "hat-middle" portion of the model, as shown in Figure 3, starting from the Teflon inserts. In other words, failure did not occur in the "skin-and-hat-perimeter" region. It originated in the skin-hat interface before migrating to the first skin ply interface. Based on this information, the model assigned VCCT interaction surfaces in these two locations, as shown in Figure 4. The middle parts in the model were broken into the hat stringer, the skin ply 1, and the skin plies 2-12, where skin ply 2 was one element layer and plies 3-12 were another layer. The length of the elements in this region (along the specimen length) was chosen to be 0.10-inches, while the width was 0.04-inches in the hat-flange damage initiation region. These dimensions were further reduced to 0.05-inches in length and 0.02-inches in width for a more refined model run. The hat and skin elements were chosen as SC8R elements in the middle region. Finally, the Aluminum load plate and potting boundary conditions were meshed coarsely with C3D8R elements and tied to the ends of the specimens.

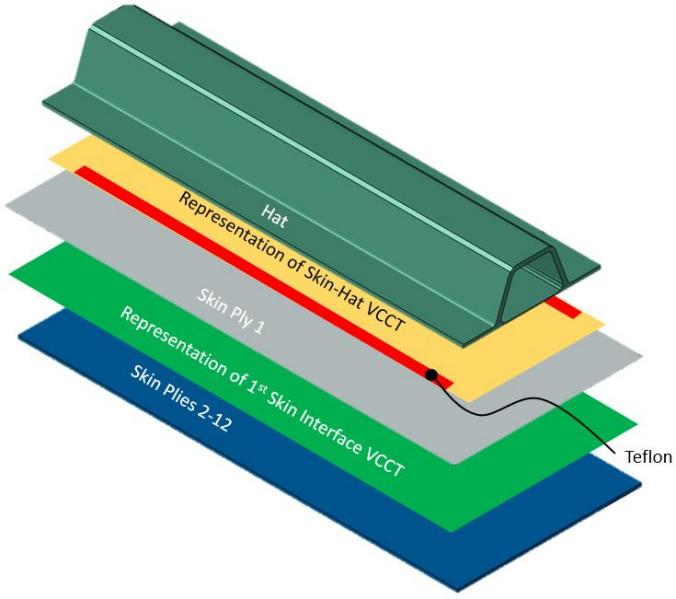

Figure 4. Exploded View of the two VCCT Assignments.

Table 2 shows the material properties used for the initiation and propagation of the crack. The values used here are slightly different from Leone et al. [14], the change accounted for model calibration. Since VCCT requires the user to define an initial crack at the start of the analysis, nodes were initially debonded between the skin and hat in the Teflon strip footprint, as shown in Figure 5. For the VCCT definition of the skin's first ply interface, a strip of the mesh 0.08-inches wide, whose center was 0.08-inches toward the center of the panel from the inside edge of the Teflon, was chosen as the initially debonded region. This best captured the test behavior of the migration from skin-hat initiation into the skin first ply debonding. The option within Abaqus to assign a nodal-based energy release rate was used, allowing a variation of toughness between the initiation and growth regions. The initiation values were assigned to nodes at the crack tips, whereas the propagation values were assigned to the remaining nodes of the VCCT surfaces. The fracture criteria used the Benzeggagh-Kenane (B-K) mixed-mode criterion. In addition, the default unstable growth tolerance of infinity and a VCCT tolerance of 0.10 were implemented. The step debonding method was chosen. Finally, a contact stabilization factor of 1.0E-6 was assigned to the interactions.

Table 2. Material Properties for VCCT

Interface	G_{IC} [in-lb/in^2]		$G_{IIC}=G_{IIIC}$ [in-lb/in^2]	η
	Initiation	Propagation		
Tape-Fabric	1.71	3.32	8.01	2.1
Tape-Tape	1.37	2.06	4.22	2.1

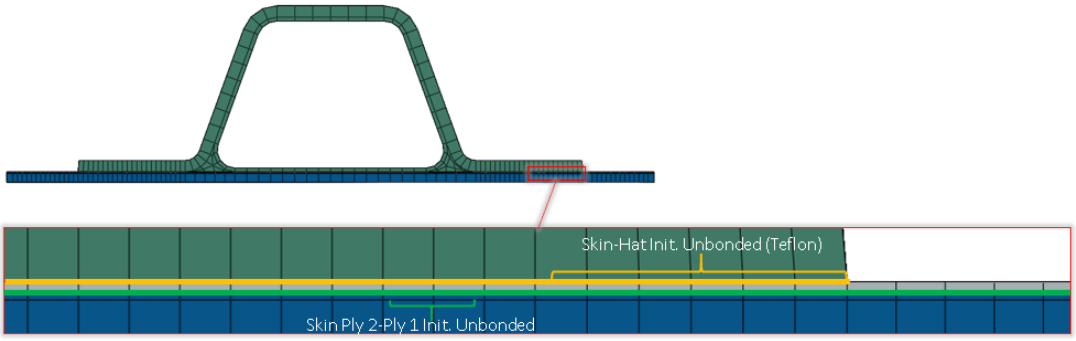

Figure 5. Detailed View of Initially Unbonded Node Regions for VCCT- Baseline Mesh for Reference

The analysis was conducted in Abaqus/Standard and Abaqus/Explicit. The Abaqus/Standard used a geometrically nonlinear analysis with unsymmetric matrix storage and solution. The analysis was displacement controlled, with zero-displacement boundary conditions assigned for the off-axis directions on both ends, and an axial compressive displacement assigned on one end, while the other end was fixed, as shown in Figure 6**Error! Reference source not found.**. Rotations were constrained due to the moment couples allowed to develop on the specimen end faces and the rigidity imparted due to the Aluminum load plates into which the specimens were potted.

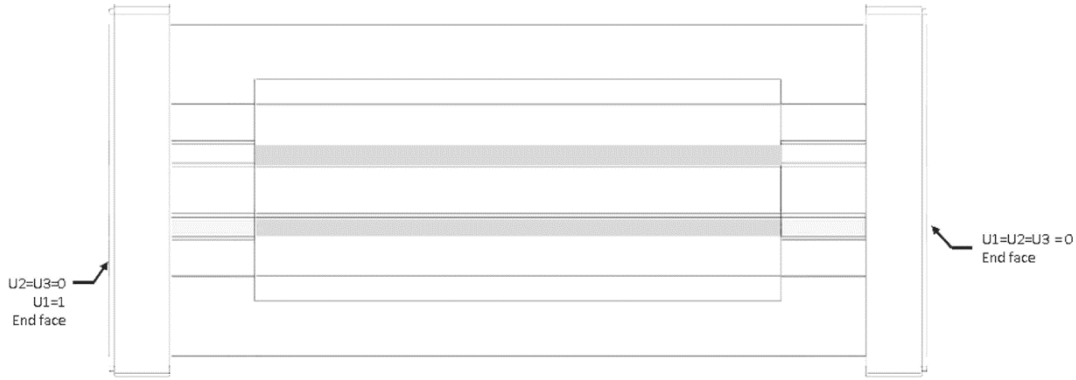

Figure 6. Abaqus/Standard model boundary conditions.

The second solution was obtained in Abaqus/Explicit. As was the case with the Abaqus/Standard, the analysis was displacement controlled with identical zero-displacement boundary conditions and a slightly different prescribed displacement. A compressive end displacement of 0.10-inches was prescribed over an interval of 10 seconds according to a “smooth step” amplitude curve, which dampens the velocity at the beginning and end of the analysis to encourage quasi-static behavior.

A linear eigenvalue buckling solution was obtained for the model. The deflections corresponding to the Type B mode shape were superimposed on the nodal coordinates of the input deck for the VCCT run with a small-scale factor (0.0015). This led to the buckling mode shape observed in the test specimens F-SCC-01 and F-SCC-04. The number of degrees of freedom (DOFs) in the baseline meshed model

was 121,000, while 211,000 DOFs in the refined mesh model. An attempt was made to regulate output times by specifying a list of time points, but a significant sensitivity to the time incrementation was discovered in the failure loads. Therefore, the time points were ultimately omitted in deference to the default incrementation in Abaqus/Standard. All models were run on an HPC with 24 CPUs. The initial analysis used an earlier Abaqus version 2021, and a numerical tolerance issue was found that was affecting the solution, as shown in Figure 7. Simulia addressed the issue and fixed it in Abaqus 2021.HF5. Therefore, Abaqus 2021.HF5 was ultimately used to run the models.

RESULTS

Undesirable behavior was observed in Abaqus release 2021 relating to nodes debonding suddenly and without a corresponding exceedance of their mixed-mode failure criteria. A code instability was discovered with the VCCT unstable growth tolerance in Abaqus version 2021. The behavior is illustrated in Figure 7, in which the bond state of the skin-hat interface is plotted. In the plots, the red color indicates debonded area while blue indicates bonded. The artificial debonding problem caused further issues, including an irregular crack front pattern and an occasional decrease in failure load. The issue was resolved in Abaqus 2021.HF5.

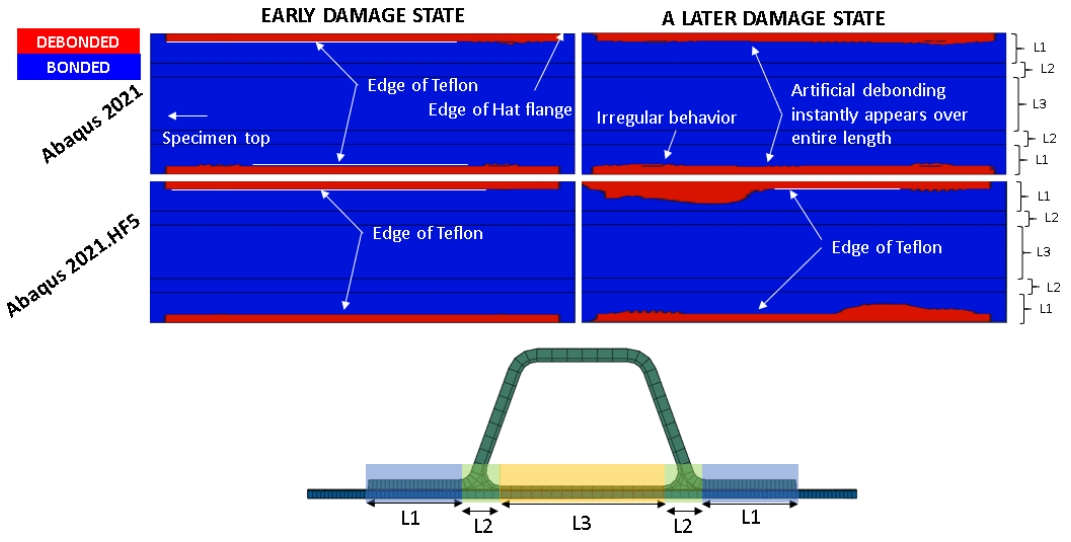

Figure 7. Comparison of Skin-Hat Debonding Behavior between Abaqus 2021 and Abaqus 2021.HF5 (seen from the hat-stiffener side).

Test specimen F-SCC-04 was unloaded at intermediate points along its loading curve to take UT scans, then reloaded to a higher load value until failure was achieved. Three scans from such pauses are shown in Figure 8. At a load of -28.6 kips, the first pause in the test, some delamination was observed between the first skin ply interface and skin-hat interface. Since the top-left location in the figure shows a small amount of skin-hat debonding only, it was believed that the damage

initiates in the skin-hat interface plane and progresses into the first skin ply interface via a series of matrix cracks in the first skin ply. By a load of -30.0 kips, the damage had progressed to a point halfway to three-quarters of the hat stiffener flange width. The damage in the test scans indicates initiation and growth from two spots at opposite ends of the specimen across the hat mid-plane.

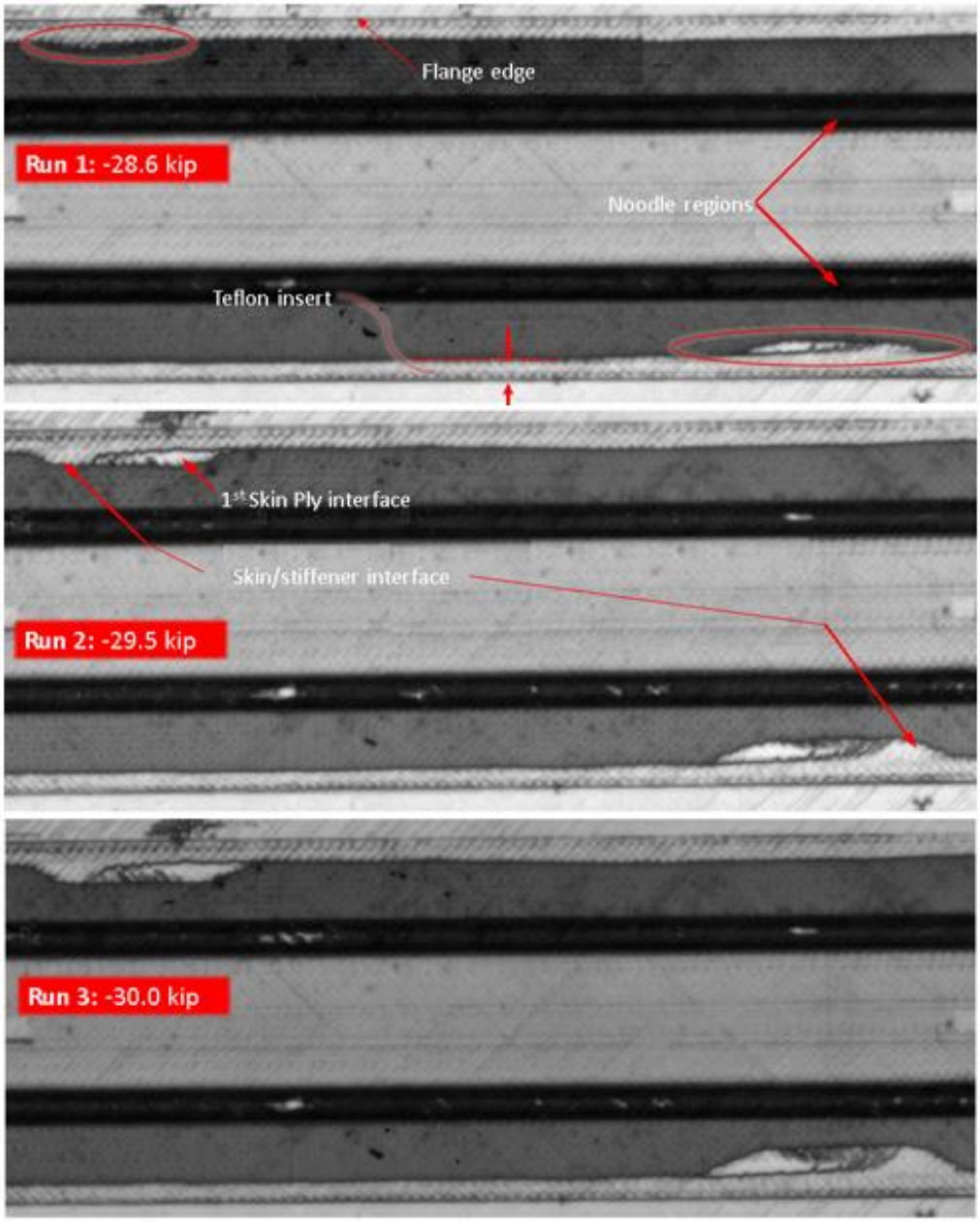

Figure 8. Specimen F-SCC-04 Stable Growth Progression UT Scans (Leone [14])

The baseline FEM run indicates damage initiation in the skin-hat interface at a load of -26.3 kips, as shown in Figure 9. These locations coincide with the buckling half-waves in the skin that deflect away from the hat flange, inducing a through-thickness tensile strain state. Debonding initiates in the first skin ply interface at a load of -28.9 kips. The peak load of the model occurs at -30.0 kips, at which the

damage has progressed up to the noodle of the hat flange. From that point, the damage becomes unstable, and the specimen experiences a release of energy manifested in a load drop. In the original analysis with specified time points, the peak load was -29.4 kips, demonstrating a 2% difference from the current analysis stemming from minor differences in time incrementation.

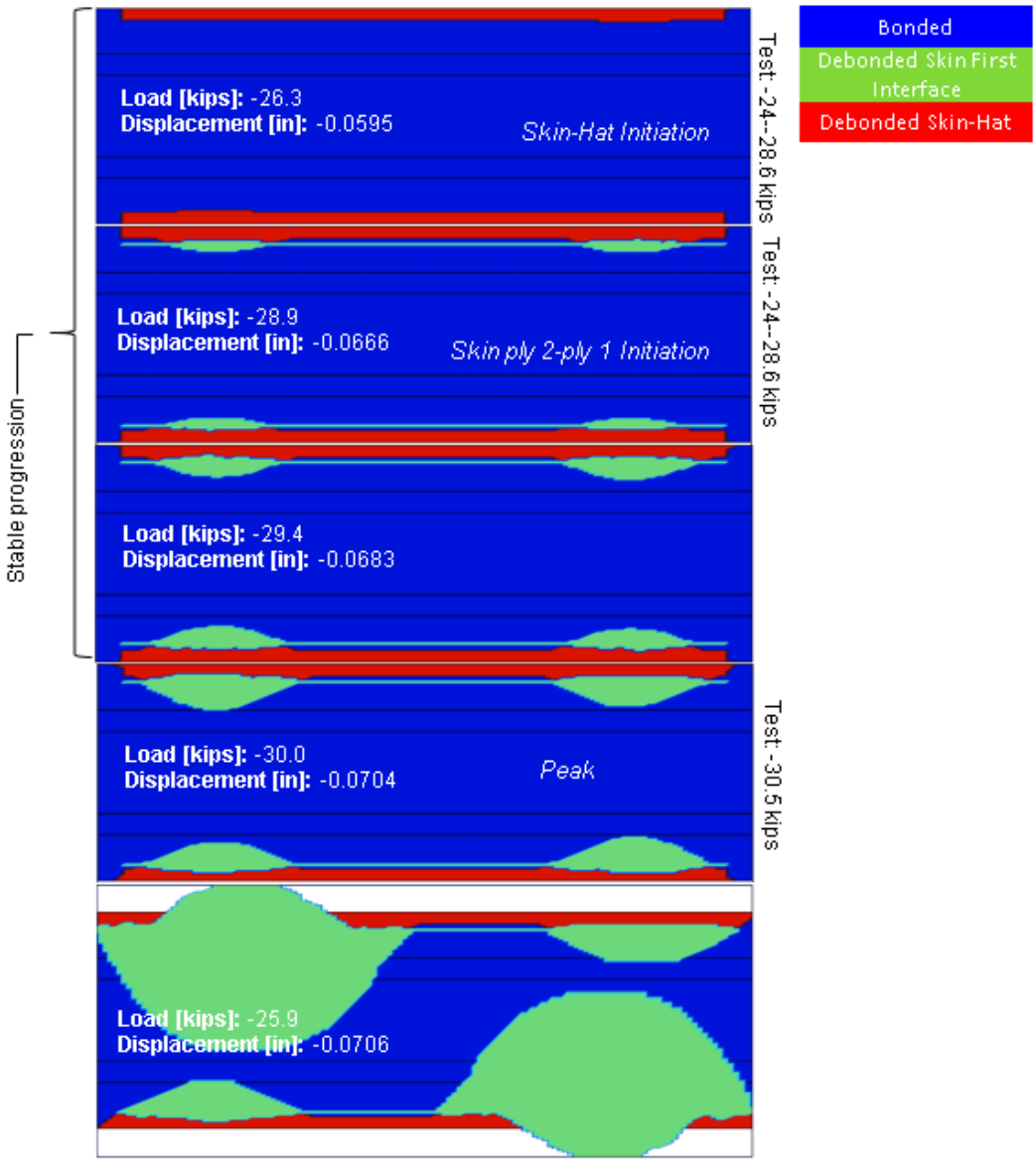

Figure 9. Debonding Progression of Baseline FEM Run in Abaqus/Standard

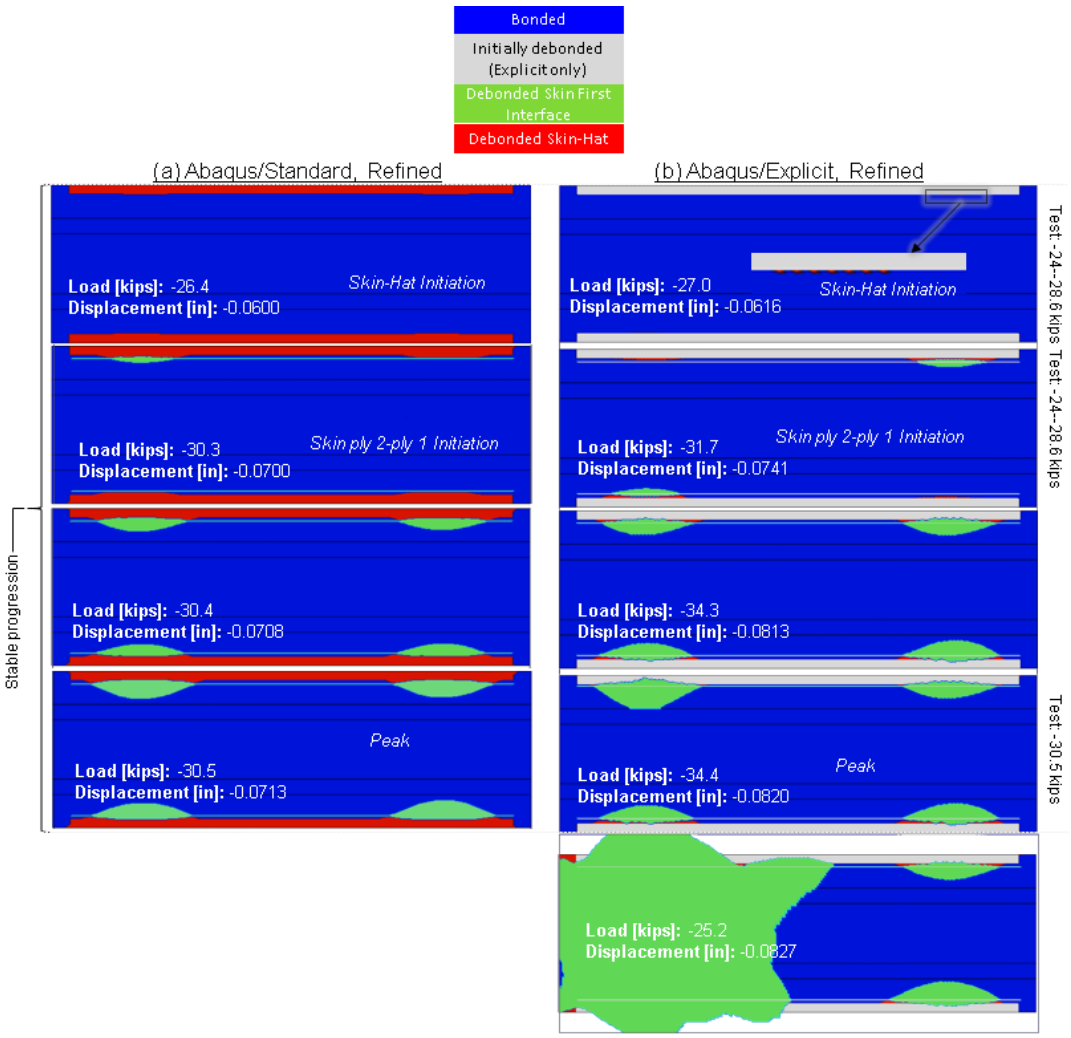

Figure 10. Debonding Progression of Refined Mesh FEM Runs in (a) Abaqus/Standard and (b) Abaqus/Explicit

Figure 10 shows the refined analyses in both Abaqus/Standard and Abaqus/Explicit. While the initiation load for the first skin ply interface is slightly higher than the test range for the implicit analysis, the peak load is captured within 1%. The explicit analysis also sees a first skin-ply interface initiation load higher than the test but also allows more stable growth to occur, resulting in a significantly higher peak load. In both solutions, delaminations are observed in each of the four locations corresponding to the skin buckling half-waves away from the hat flange.

As shown in Table 3, the baseline mesh run in Abaqus/Standard captures all primary load values within 2% of the test data. Since the buckling of the panel was not an instantaneous event but happened over a range of 2-3 kips, a precise load is not given, but all FEM runs sees buckling happen around 15 kips as in the test. In addition, the refined mesh run in Abaqus/Standard captures the peak load but has a slightly higher error of 6% for the skin ply 2-ply 1 interface initiation. The refined mesh run in Abaqus/Explicit sees an 11-13% error in the skin ply 2-ply 1 interface initiation and peak load.

Table 3. Test and FEM Loads Comparison

	Test	Baseline Standard		Refined Standard		Refined Explicit	
	Comp. Load [kips]	Comp. Load [kips]	% Err	Comp. Load [kips]	% Err	Comp. Load [kips]	% Err
Buckling	~15	~15	~0.0%	~15	~0.0%	~15	~0.0%
Skin-Hat Initiation	24-28.6	26.3	--	26.4	--	27	--
Skin 1st Interface Initiation	24-28.6	28.9	+1.0%	30.3	+5.9%	31.7	+10.8%
Peak	30.5	30	-1.6%	30.5	0.0%	34.4	+12.8%

Figure 11 is a plot of the compressive axial load versus displacement, indicating a mean pre-buckled stiffness in the test data of 4.4E+05 lb/in and a post-buckled stiffness of 3.8E+05 lb/in. The FEM exhibits a slightly higher stiffness overall, where the mean pre-buckled stiffness is 4.7E+05 lb/in and the post-buckled 4.0E+05 lb/in. Similar behavior was observed by Leone et al. [14]. This led to a 5-7% error in the overall stiffness between the two datasets, which is depicted graphically in the load versus displacement plot where the FEM curves overlay well with the test curve adjusted to a 5% stiffness increase. The slight stiffness mismatch could be due to axial deflection outside of the test article stemming from compliance in the load train and introduction, and it did not affect the failure loads. The knee in the curve corresponding to the panel buckling matches well between the test and FEM curves. The skin-hat initiation loads for all models are within the test data range. However, the skin ply 2-ply 1 initiation loads are between 1% and 11% above the upper end of the test range. The baseline and refined models run in Abaqus/Standard show excellent agreement (within 2%) of the tested peak load. The Abaqus/Explicit run has a longer period of stable growth and delays failure until 34.4 kips, 13% higher than observed in the test.

The buckling of the panel in the FEM was evaluated by plotting the compressive load versus out-of-plane displacements at the six half-wave peak locations on the skin in Figure 12. A clear knee in this curve is also apparent at 15 kips, with some semi-buckled mode shape formation prior, between 10 and 15 kips, which is an artifact of the small buckling shape superimposition on the model to promote Type B buckling. As expected, the four locations, 1L, 1R, 3L, and 3R, indicated on the plot correspond to the lengthwise locations of damage experienced in the skin-hat and skin ply 2-ply 1 interface.

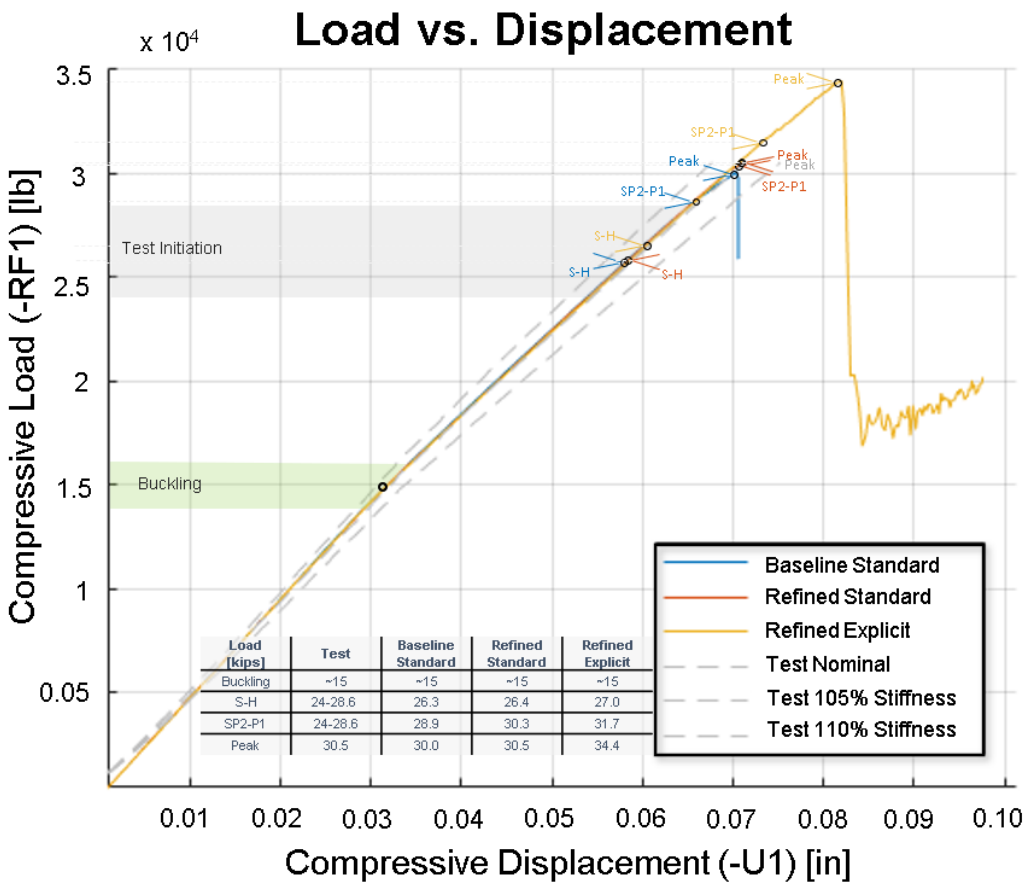

Figure 11. The load-displacement curve for stiffened post-buckled panels.

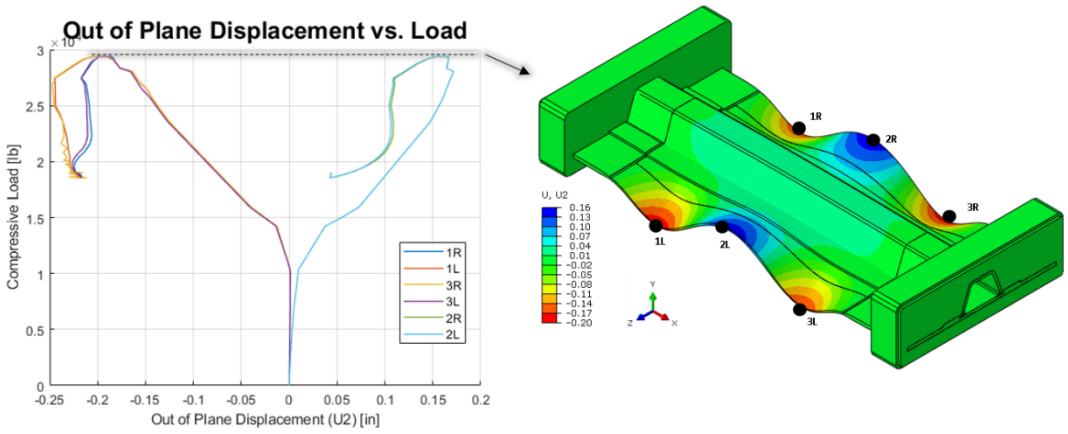

Figure 12. Load vs. Out-of-Plane Displacement

CONCLUSIONS

The model verification of a single hat-stiffener panel model with a Teflon insert was completed using multiple VCCT definitions in Abaqus to capture damage initiation (beyond the embedded damage) and progression under a post-buckled state. Although the peak loads were within 2% for the implicit analysis, it is not fully predictive on its own because of pre-determined inputs. The primary inputs required were the location of initial damage and the superposition of the eigenvalue buckling mode shape on the model. With these limitations in mind, the global-to-local modeling approach successfully captured the pre-buckled behavior of the panel, the buckling load, the load initiation, and the peak load compared with the test data. The stiffness was within 8% of the average test value. In addition, the model was able to capture the location of damage initiation between the skin-stringer panel and its migration between the skin-stiffener interface and the skin's ply1-ply2 interface.

ACKNOWLEDGMENTS

The authors want to thank the Office of the Naval Research for their support under Award No. N00014-21-C-1007. Also, the authors are grateful to the NASA ACP Progressive Damage Analysis Cooperative Research Team for granting permission to use the experimental data completed under Award No. NNL09AA00A.

REFERENCES

1. Degenhardt R, Castro SGP, Arbelo MA, Zimmerman R, Khakimova R, Kling A., "Future structural stability design for composite space and airframe structures," Thin-Wall Structures, 2014, Vol 81(7).
2. Hao P, Wang B, Tian K, Li G, Du K, Luan Y., "Integrated optimization of hybrid stiffness stiffened shells based on sub-panel elements," Thin-Wall Structures, 2016, Vol 103.
3. Gliszczynski A, Kubiak T., "Progressive failure analysis of thin-walled composite columns subjected to uniaxial compression," Composite Structures, 2017, Vol 169.
4. Pietropaoli E, Riccio A, "A global/local finite element approach for predicting interlaminar and intralaminar damage evolution in composite stiffened panels under compressive load," Appl Compos Mater, 2011, Vol 18(2).
5. Gong Y, Zhang B, Hallett SR., "Delamination migration in multidirectional composite laminates under mode I quasi-static and fatigue loading," Compos Struct, 2018; Vol 189.
6. Gong Y, Zhao L, Zhang J, Wang Y, Hu N., "Delamination propagation criterion including the effect of fiber bridging for mixed-mode I/II delamination in CFRP multidirectional laminates," Compos Sci Technol, 2017, Vol 151.
7. Bisagni C, Vescovini R, Davila CG. "Development of a single-stringer compression specimen for the assessment of damage tolerance of postbuckled structures." J Aircraft, 2011, Vol 48(2).
8. Anyfantis KN, Tsouvalis NG. "Post buckling progressive failure analysis of composite laminated stiffened panels." Appl Compos Mater, 2012, Vol 19(3-4).

9. De Carvalho NV, Mabson GE, Krueger R, Deobald LR. “A new approach to model delamination growth in fatigue using the Virtual Crack Closure Technique without re-meshing.” Eng Fract Mech, 2019, Vol 222.

10. Mabson GE, Deobald LR, Dopker B, Hoyt DM, Baylor JS, Graesser DL. “Fracture interface elements for static and fatigue analysis.” Proceedings of 16th international conference on composite materials (ICCM16), Kyoto, 2007.

11. Di Memmo I, Bisagni C. “Fatigue simulation for damage propagation in composite structures.” Proceedings of 32nd technical conference of the American Society for Composites, West Lafayette, 2017, No. 135472.

12. Raimondo A, Doesburg SA, Bisagni C. “Numerical study of quasi-static and fatigue delamination growth in a post-buckled composite stiffened panel.” Compos B Eng, 2019.

13. Camanho PP, Davila CG, de Moura M. “Numerical simulation of mixed-mode progressive delamination in composite materials.” J Compos Mater, 2003, Vol 37.

14. Leone, FA, Song K, Rose CA, Jackson WC, “Progressive Damage Analysis of Post-Buckled Stiffened Panels under Static Compressive Loading,” AIAA SciTech Forum, 6-10 January 2020, Orlando, FL.

15. Leone, FA, Song K, Johnston W, Rose CA, Jackson WC, Kosztowny CJ, Davila CG, “Test/Analysis Correlation of Damage States in Post-buckled Stiffened Validation Building Block Specimens,” Proceedings of 34th technical conference of the American Society for Composites, 2019, No. 28086.